

## Electronic Supplementary Information (ESI)

### Strain and pH facilitated artificial photosynthesis in monolayer MoS<sub>2</sub> nanosheet

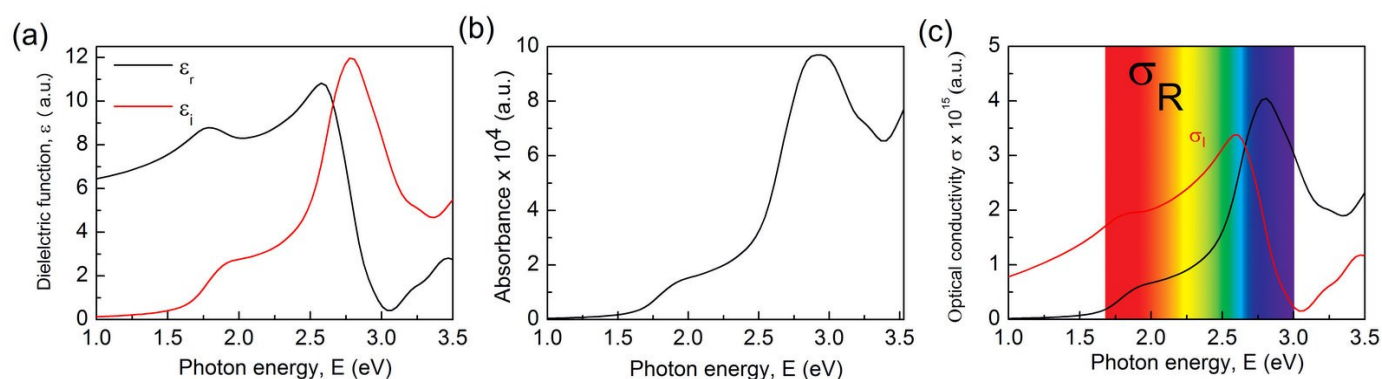


Figure S1 (a) Real  $\epsilon_1(\omega)$  and imaginary  $\epsilon_2(\omega)$  part of the frequency dependent dielectric function (b) Absorption spectra,  $\alpha_{abs}$ , (c) Real,  $\sigma_r(\omega)$  and imaginary,  $\sigma_i(\omega)$  part of optical conductivity in pristine unstrained single layer MoS<sub>2</sub>

The calculated optical conductivity correctly reproduces all main features measured experimentally [*Appl. Phys. Lett.*, 2015, **107**, 83103] and calculated theoretically [*J. Mater. Chem. C*, 2016, **4**, 8822–8828] based on the empirical Sellmeier equation between refractive index and incident photon energy

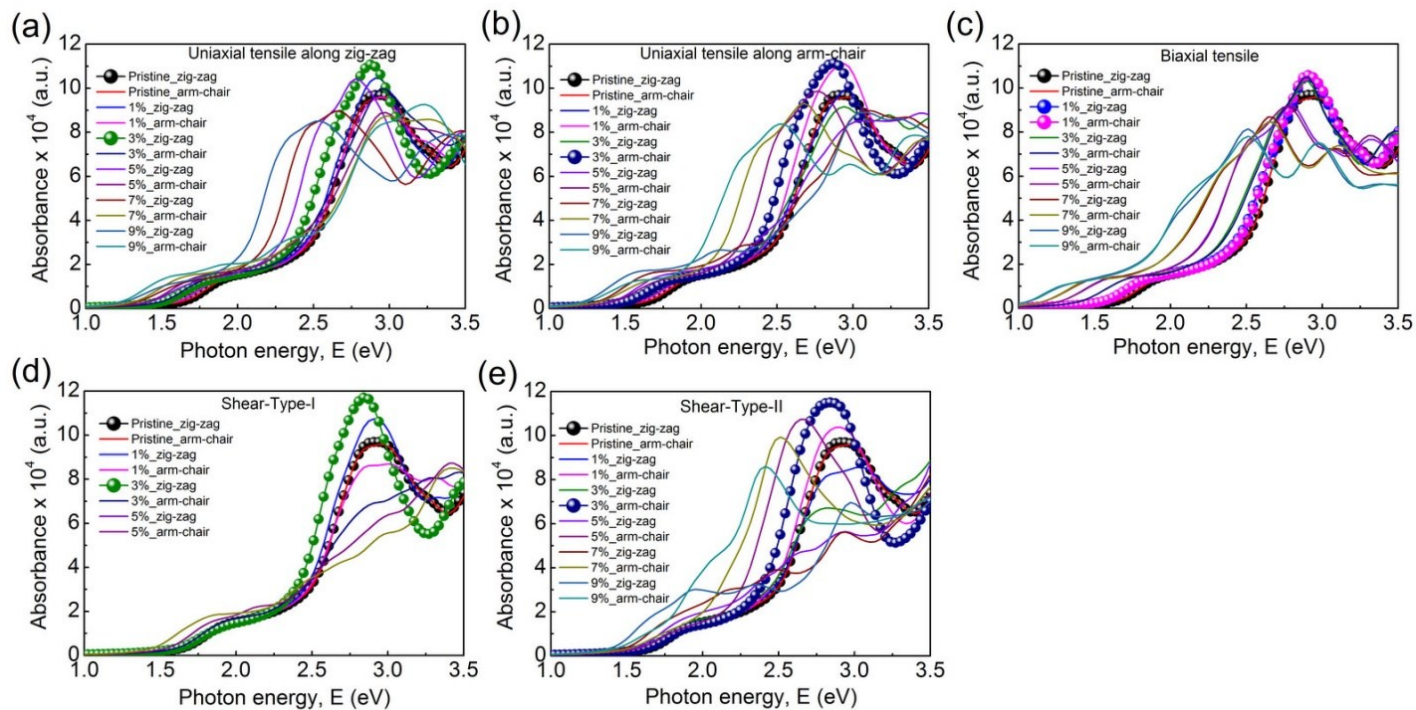


Figure S2 Variation in the absorbance spectra with different kinds of applied mechanical strain

Absorbance is direction dependent. Pristine\_zig-zag and Pristine\_arm-chair represent absorbance along the zig-zag and arm-chair directions in unstrained condition. When 1% tensile strain is applied, absorbance along both the zig-zag and arm-chair directions change. In Fig. (a), for 1% uniaxial tensile strain applied along the zig-zag direction, the labels 1% zig-zag and 1% arm-chair represent absorbance along the zig-zag and arm-chair directions respectively. Likewise, in Fig. (b), for 1% uniaxial tensile strain applied along the arm-chair direction, the labels 1% arm-chair and 1% zig-zag represent absorbance along the arm-chair and zig-zag directions respectively. In Fig. (c), for 1% biaxial tensile strain, 1% zig-zag and 1% arm-chair correspond to absorbance along the zig-zag and arm-chair directions respectively.

The redshift in absorbance peaks with the application of uniaxial and biaxial tensile strain agrees with the PL observed experimentally [Nano Lett., 2013, 13, 3626–3630 & Nano Lett., 2016, 16, 5836–5841]

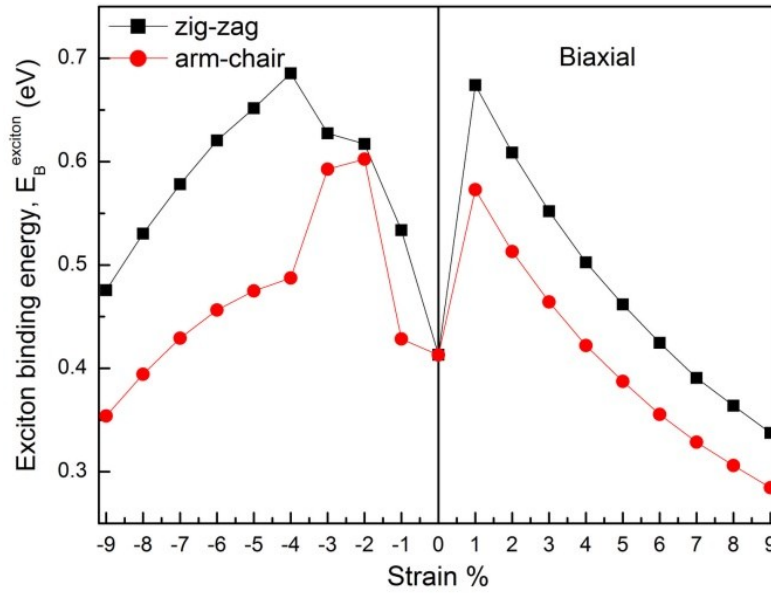


Figure S3 Variation in excitonic binding energy with biaxial strain applied on to ML-MoS<sub>2</sub> nanosheet

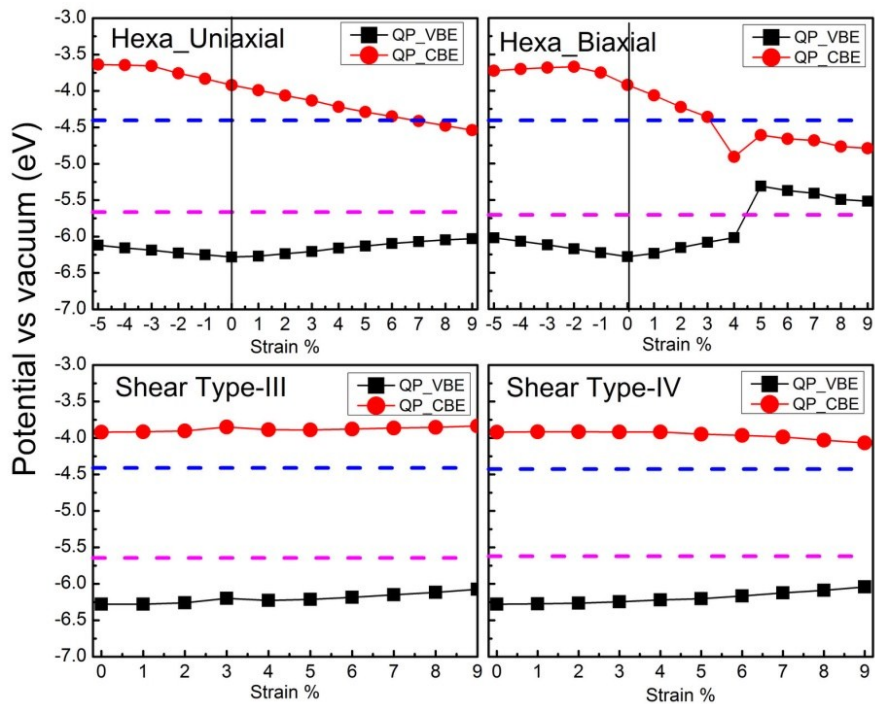


Figure S4 Variation in valence and conduction band edges with the application of different types of strain in monolayer MoS<sub>2</sub> studied in a supercell with hexagonal symmetry for solar water splitting

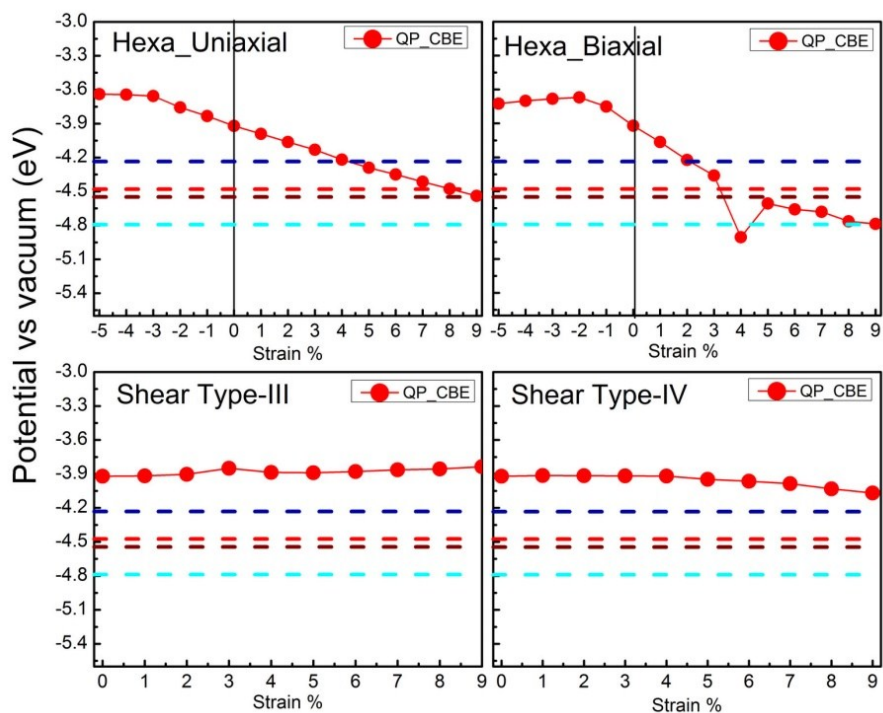


Figure S5 Variation in the valence and conduction band edges with the application of different types of strain in single layer MoS<sub>2</sub> studied in a supercell with hexagonal symmetry for CO<sub>2</sub> reduction

**Table ST1** Electrode potential (EP) for reducing CO<sub>2</sub> to different fuel precursors/fuel relative to Normal Hydrogen Electrode (NHE) potential at pH = 0, 7 and 14

System	EP(V) at pH=0	EP(V) at pH=7	EP(V) AT pH=14
CO <sub>2</sub> to CO <sub>2</sub> <sup>-</sup>	-1.4856	-1.9	-2.3144
CO <sub>2</sub> to CO	-0.103	-0.52	-0.93
O <sub>2</sub> to H <sub>2</sub> O	1.234	+0.82	0.4052
H <sup>+</sup> to H <sub>2</sub>	0	-0.41	-0.82
CO <sub>2</sub> to HCOOH	-0.199	-0.61	-1.02
CO <sub>2</sub> to HCHO	-0.066	-0.48	-0.895
CO <sub>2</sub> to CH <sub>3</sub> OH	0.03	-0.38	-0.79
CO <sub>2</sub> to CH <sub>4</sub>	0.169	-0.24	-0.65

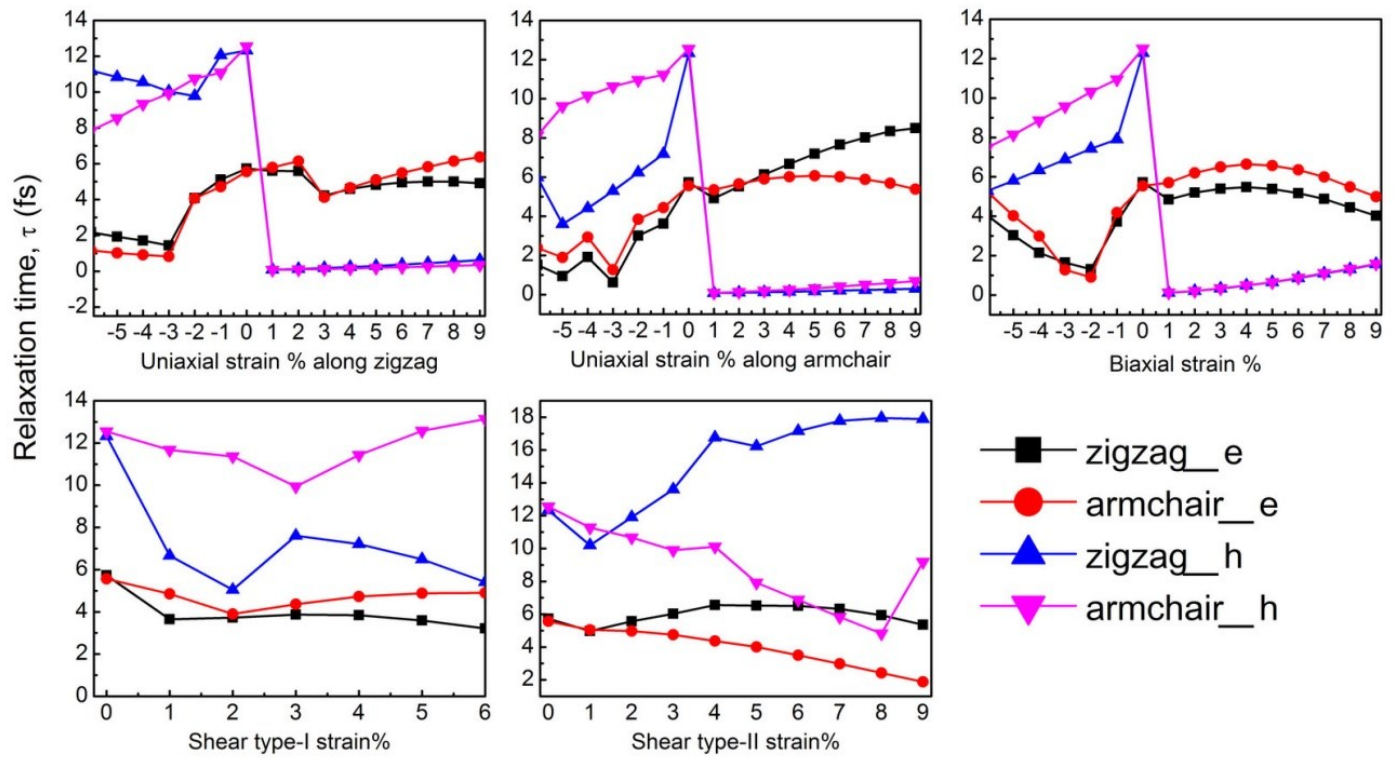


Figure S6 Variation in the relaxation time of the charge carriers along the zig-zag (zz) and arm-chair (ac) direction with mechanical strain of different types applied on to monolayer MoS<sub>2</sub> nanosheet